Central Lancashire Online Knowledge (CLoK)

Title	Effect of Mesh Phasing on the Transmission Efficiency and Dynamic Performance of Wheel Hub Planetary Gear Sets
Type	Article
URL	https://clok.uclan.ac.uk/32120/
DOI	https://doi.org/10.1177/0954406217737327
Date	2018
Citation	Fatourehchi, Ehsan, Mohammad Pour, Madhi, King, Paul D., Rahnejat, Homer, Trimmer, G, Williams, A and Womersley, B (2018) Effect of Mesh Phasing on the Transmission Efficiency and Dynamic Performance of Wheel Hub Planetary Gear Sets. Proceedings of the Institution of Mechanical Engineers, Part C: Journal of Mechanical Engineering Science, 232 (19). pp. 3469-3481. ISSN 0954-4062
Creators	Fatourehchi, Ehsan, Mohammad Pour, Madhi, King, Paul D., Rahnejat, Homer, Trimmer, G, Williams, A and Womersley, B

It is advisable to refer to the publisher's version if you intend to cite from the work.
https://doi.org/10.1177/0954406217737327

For information about Research at UCLan please go to http://www.uclan.ac.uk/research/

Original Article

Effect of mesh phasing on the transmission efficiency and dynamic performance of wheel hub planetary gear sets

Ehsan Fatourehchi[1], Mahdi Mohammadpour[1], Paul D King[1], Homer Rahnejat[1], Gareth Trimmer[2], Alan Williams[2] and Robert Womersley[2]

Abstract
Transmission efficiency and refinement of planetary wheel hub gearing system are key design attributes for heavy and off-highway vehicles. Reduction of power loss, directly leading to the development of new generation ECO-axles requires analysis of gear contacting conditions for lubricated conjunctions to determine frictional performance. This is also affected by gear dynamics, which is a prerequisite for assessment of noise, vibration and harshness performance. Therefore, a combined tribo-dynamic analysis is essential. There is a dearth of such holistic analysis, particularly for the case of wheel hub planetary systems. The paper presents such an analysis, which has not hitherto been reported in literature. The inexorable interplay of transmission efficiency and noise, vibration and harshness refinement is demonstrated. The key attributes of noise, vibration and harshness refinement and transmission efficiency can pose contrary requirements and near-optimal conditions can be highlighted by mesh phasing of gearing contacts, thus alleviating the need for more complex gear teeth modifications entailing prohibitive manufacturing costs.

Introduction

Planetary gears have a wide range of application, including in vehicular drive trains. They provide a wide range of transmission ratios. There are a number of major advantages for planetary gears, including better transmission efficiency when compared with fixed axes transmissions.[1] Planetary gears are generally considered to be quieter than their alternatives.[2] These relative advantages depend heavily on the application and working conditions. One of these applications is the wheel hub planetary set, with particular application in the off-highway and heavy duty vehicles. The main design concerns in these cases are the transmission efficiency and noise, vibration and harshness (NVH) refinement. This is the application of interest here.

On the issue of NVH characteristics, mesh phasing of planets is the approach usually undertaken, as reported by Kahraman,[3] who developed a dynamic model for the analysis of mesh phasing. He included all the six rigid body degrees of freedom (DOF) of the gearing system, showing that their higher harmonic excitations preclude the chance of eliminating the transmission error under static or dynamic conditions. Ambarisha and Parker[4] compared the non-linear dynamics of spur planetary gears in a two-dimensional lumped-parameter model. Comparing the results with a two-dimensional finite element model was provided. The study validated the effectiveness of lumped parameter modelling for the analysis of planetary gear dynamics. Ambarisha and Parker[5] used the analytical model to investigate the effect of mesh phasing between the planets in order to suppress certain harmonics of the modal response.

[1]Wolfson School of Mechanical, Electrical and Manufacturing Engineering, Loughborough University, Loughborough, UK
[2]JCB Transmission, Wrexham Industrial Estate, Wrexham, UK

Corresponding author:
Mahdi Mohammadpour, Wolfson School of Mechanical, Electrical and Manufacturing Engineering, Loughborough University, Loughborough LE113TU, UK.
Email: m.mohammad-pour@lboro.ac.uk

Another approach to palliate some sources of excitation as well as improving transmission efficiency is through modifying the profiles of the teeth. Bahk and Parker[6] studied the effect of modified tooth profile on vibrations of spur planetary gears. They established an analytical approach to determine the effect of tooth profile on the sun–planet and planet–ring contacts. This was a two-dimensional lumped parameter model of a spur planetary gear with modified tooth profile. The results showed that some additional excitations are induced by modified tooth profiling, which can be represented as the product meshing stiffness and the profile modification function.

On the issue of transmission efficiency, there is some limited reported work. These include the experimental measurement of planetary gear power loss by Talbot et al.[7] Experiments were carried out for both loaded and unloaded gear conditions, showing a reduction in power loss with a reduced number of planets and increased bulk lubricant temperature under unloaded conditions. Under loaded conditions, a decrease in lubricant temperature and improved contact surface finish decreased the mechanical power loss.

Transmission efficiency and NVH refinement of gear trains are inexorably coupled through contact friction in all forms of gearing systems, meaning that ideally a tribo-dynamics model of the system would be required for any detailed analysis.[8–10] Therefore, it is essential to provide predictive tools for design purposes, which would integrate system dynamics with lubricated contacts. This approach enables the determination of the influence of key parameters upon transmission efficiency and NVH performance.[11] Mohammadpour et al.[12] presented a tribo-dynamic model for the planetary gear sets, using this approach. Their results showed that NVH

refinement worsens with reduced frictional power loss, indicating the critical role of friction as an energy sink, expending the excessive applied power, which is often the case in modern powertrain systems. The link between friction in lubricated contacts and various NVH phenomena is now fairly well understood, such as in gear rattle[13–15] and rear axle whine.[16]

A tribo-dynamic model of off-highway wheel hub planetary gears is reported here. The dynamic model takes into account the torsional DOF of the sun, planet, ring and the carrier, coupled with an analytical lubricated contact model of meshing teeth pairs. Therefore, the model enables simultaneous predictions for NVH performance as well as evaluation of power losses and transmission efficiency. Mesh phasing of gear pairs is investigated to ascertain its effect upon both NVH refinement as well as transmission efficiency under representative in-field operating conditions. An integrated tribo-dynamic analysis is developed. Such a study for planetary wheel hub gearing of off-highway vehicles has not been reported in literature.

Wheel hub configuration

Figure 1(a) shows the power flow from the gearbox to the wheel hub gears. The transmission ratio, torque and speed values are presented at the different stages of the axle system. This load condition represents an example of top-speed and zero-gradient condition for a nine-tonne vehicle. Figure 1(b) shows the wheel hub planetary gear system. In the studied system, the sun gear is attached to the input shaft, the ring gear to the housing and the power is transmitted to the wheels through the carrier. The planetary system consists of three planets.
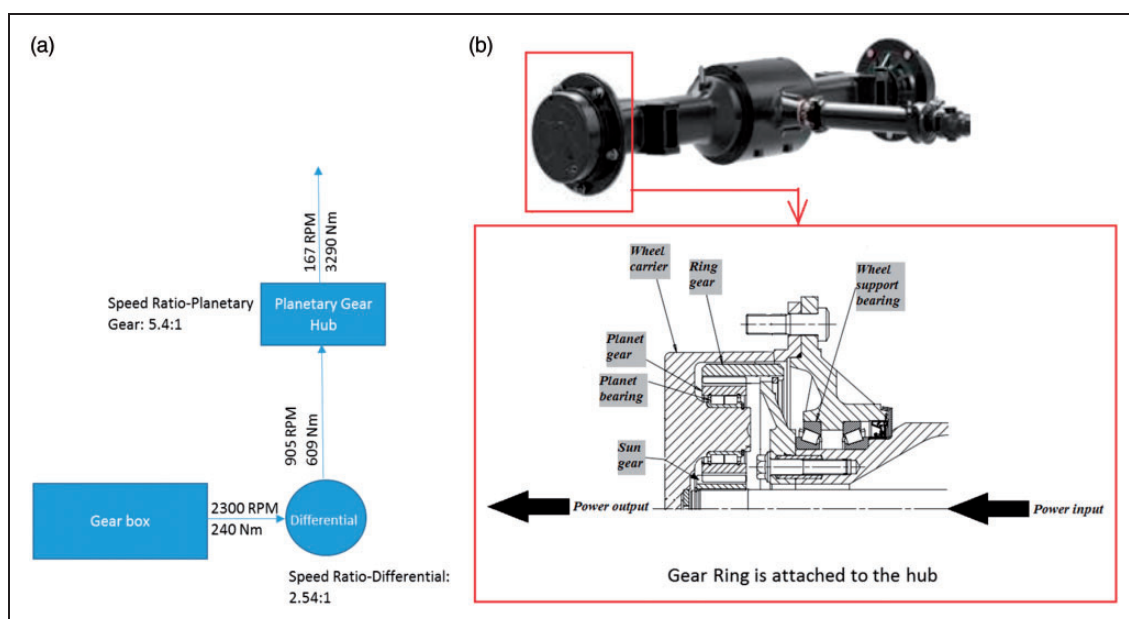
Figure 1. (a) Power flow from the gearbox to the wheel hub and (b) schematic representation of the planetary wheel hub.

The numerical tribo-dynamics model

Dynamic model

To model the dynamics of the planetary systems, different approaches have been proposed. Chen and Shao,[17] and Sun and Hu[18] coupled both lateral and torsional DOFs in modelling the dynamics of planetary system. The same approach is reported by Spitas and Spitas[19] to model a single-stage spur gear. The purpose of considering lateral vibration is to capture the interaction with the bearings and gearbox foundation.

In this study, since the main focus is on the suppression of the internal excitation due to the gear meshing, the lateral motions of the gears[20] are not taken into account. Therefore, the dynamics model comprises six torsional DOFs. These comprise torsional DOF of the sun gear, the ring gear, the carrier and the three planet gears. Figure 2 shows the devised model.

The equations of motion are

$$I_s\ddot{\theta}_s + \sum_{i=1}^{3}(DTE_{spi}k_{spiT}(T_s, \theta_s + \emptyset_{spi})$$
$$+ D\dot{T}E_{spi}c_{spiT}) = T_s$$
$$I_r\ddot{\theta}_r + \sum_{i=1}^{3}(DTE_{rpi}k_{rpiT}(T_r, \theta_s + \emptyset_{rpi})$$
$$+ D\dot{T}E_{rpi}c_{rpiT}) = T_r$$
$$I_c\ddot{\theta}_c + \sum_{i=1}^{3}(DTE_{spi}k_{spiT}(T_s, \theta_s + \emptyset_{spi}) + D\dot{T}E_{spi}c_{spiT}$$
$$+ DTE_{rpi}k_{rpiT}(T_r, \theta_s + \emptyset_{rpi}) + D\dot{T}E_{rpi}c_{rpiT}) = T_c$$
$$I_{p1}\ddot{\theta}_{p1} + (DTE_{sp1}k_{sp1T}(T_s, \theta_s + \emptyset_{spi}) + D\dot{T}E_{sp1}c_{sp1T}$$
$$- DTE_{rp1}k_{rp1T}(T_r, \theta_s + \emptyset_{rpi}) - D\dot{T}E_{rp1}c_{rp1T}) = 0$$

$$I_{p2}\ddot{\theta}_{p2} + (DTE_{sp2}k_{sp2T}(T_s, \theta_s + \emptyset_{spi}) + D\dot{T}E_{sp2}c_{sp2T}$$
$$- DTE_{rp2}k_{rp2T}(T_r, \theta_s + \emptyset_{rpi}) - D\dot{T}E_{rp2}c_{rp2T}) = 0$$
$$I_{p3}\ddot{\theta}_{p3} + (DTE_{sp3}k_{sp3T}(T_s, \theta_s + \emptyset_{spi}) + D\dot{T}E_{sp3}c_{sp3T}$$
$$- DTE_{rp3}k_{rp3T}(T_r, \theta_s + \emptyset_{rpi}) - D\dot{T}E_{rp3}c_{rp3T}) = 0$$

$$(1)$$

where, $i = 1 - 3$ indicate the number of planet branches.

The dynamic transmission error (DTE) is due to the localised contact deformation of the teeth as well as the global bending of the gear teeth and rim. This parameter is used as a measure of NVH refinement. For the various gears, it is obtained as

$$DTE_{spi} = fa(\theta_s/r_p - \theta_{pi} - \theta_c r_c/r_p) \quad (2)$$

$$D\dot{T}E_{spi} = fa(\dot{\theta}_s/r_p - \dot{\theta}_{pi} - \dot{\theta}_c r_c/r_p) \quad (3)$$

$$DTE_{rpi} = fa(\theta_{pi} - \theta_r r_r/r_p - \theta_c r_c/r_p) \quad (4)$$

$$D\dot{T}E_{rpi} = fa(\dot{\theta}_{pi} - \dot{\theta}_r r_r/r_p - \dot{\theta}_c r_c/r_p) \quad (5)$$

$\emptyset_{rpi}$ and $\emptyset_{spi}$ are the differences in the meshing phase of each planet with respect to the ring or the sun gear. The phase difference in the meshing is presented in Figure 3.

For the ring gear, the equation of motion is constrained (disregarded). The corresponding terms in equations (2) to (5) are also ignored.

The backlash in teeth pair conjunctions should be taken into account. It introduces system non-linearity.
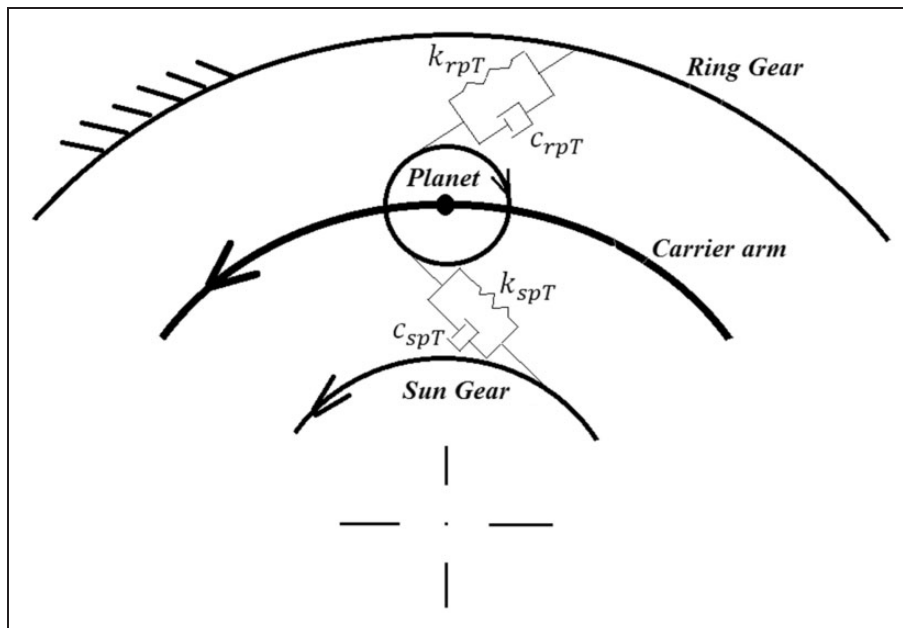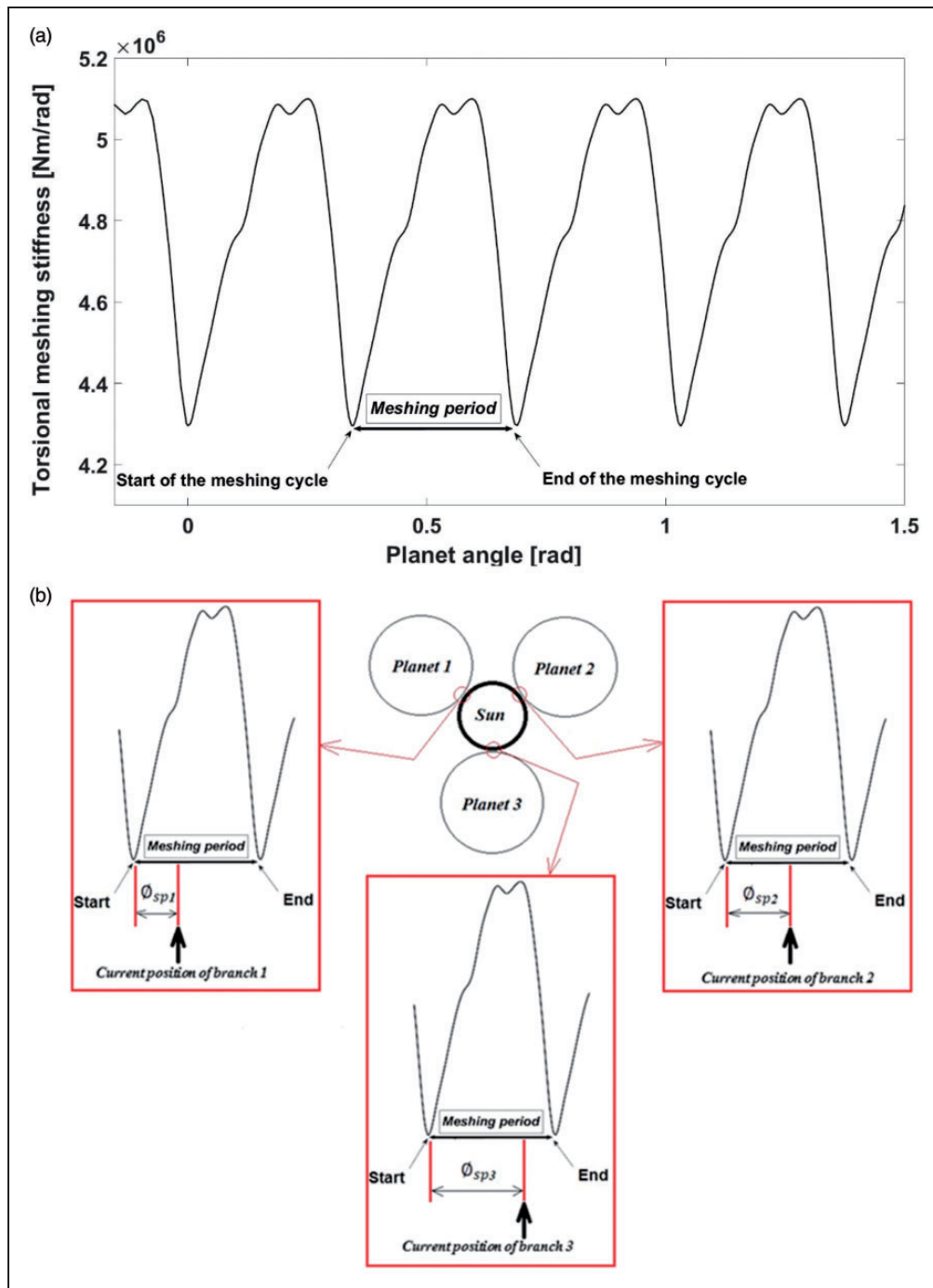

Figure 2. The gear set model.

Figure 3. (a) Meshing stiffness of the ring-planet contact obtained through TCA. (b) Schematic representation of gear phasing in different planetary branches.

This leads to teeth pair impact and separation in the vicinity of system resonances. The backlash is given by piecewise linear relationships:

$$\begin{cases} fa = 1 & 0 < DTE \text{ or } DTE < -r_p B \\ fa = 0 & -r_p B < DTE < 0 \end{cases} \quad (6)$$

Meshing stiffness

In order to obtain more accurate results, recently the planetary transmission systems are modelled using various computational approaches, including finite element analysis (FEA). Iglesias et al.[21,22] developed a finite element model to determine the contact meshing stiffness. The same approach is reported by Oyague[23] utilizing the SIMPACK software.

The gear pairs used for the off-highway wheel hubs are spur gears. In order to obtain the nonlinear load variable meshing stiffness at all the mesh points in the current study, the commercial FEA-based tooth contact analysis (TCA) package, reported by Vijayakar[24] and Xu and Kahraman[25] is used.

The TCA model is also used to calculate instantaneous contact geometry, and the rolling and sliding contact velocities[8,12,26] to determine contact friction of meshing gear teeth pairs. All the data obtained through TCA are expressed as an eighth-order Fourier series with respect to the planet angle. Furthermore, in order to consider the effect of applied torque on the meshing stiffness, the TCA model is run for a range of applied torques. Then, the coefficients of Fourier function of the meshing stiffness are expressed as functions of applied torque. Figure 3 shows a typical meshing stiffness of the ring-planet contact obtained through TCA.

It is important to include material damping due to hysteresis.[27,28] The damping coefficient for a single meshing pair is[28]

$$c = \frac{0.009k}{f_m} \tag{7}$$

where, f_m is the meshing frequency.

The tribological model

Gears typically operate under mixed regime of lubrication (elastohydrodynamics and asperity interactions). Therefore, the mechanisms underlying generated friction are due to viscous shear of a thin lubricant film as well as any direct interaction of asperities on the counter face surfaces of gear teeth flanks. Thus, the total friction becomes

$$f = f_v + f_{bo} \tag{8}$$

The Greenwood and Tripp[29] method is used to determine the contribution due to boundary interaction of rough meshing surfaces, assuming that asperity heights on the counter face surfaces follow a Gaussian distribution. A small fraction of the instantaneous contact load is supported by these ubiquitous asperities under mixed regime of lubrication. This is indicated by the Stribeck's lubricant film parameter: $\lambda = \frac{h_{c0}}{\sigma} \leqslant 3$, where σ is the composite root mean square roughness of the counter face rough surfaces. Then the load supported by contact of these asperities becomes[29]

$$W_a = \frac{16\sqrt{2}}{15}\pi(\xi\beta\sigma)^2\sqrt{\frac{\sigma}{\beta}}E'AF_{5/2}(\lambda) \tag{9}$$

where, $F_{5/2}(\lambda)$ is a statistical function for the Gaussian distribution of asperities heights. For steel surfaces, it is represented by a fifth-order polynomial fit as[30]

$$F_{5/2}(\lambda) = \begin{cases} \begin{Bmatrix} -0.004\lambda^5 + 0.057\lambda^4 - 0.296\lambda^3 \\ +0.784\lambda^2 - 1.078\lambda + 0.617; \end{Bmatrix} & for\ \lambda \leqslant 3 \\ 0; & for\ \lambda > 3 \end{cases} \tag{10}$$

For steel surfaces, the roughness parameter $\xi\beta\sigma$ is in typically: 0.03–0.07. The ratio σ/β is a representation of the average asperity slope,[30] which is in the range 10^{-4}–10^{-2}.[30] These parameters are measured using white light interferometer, Alicona with a vertical resolution of 1 Nm and horizontal resolution of 0.175 μm. The results of measurements for 10 sampled area of teeth flanks yield: $\xi\beta\sigma = 0.055$ and $\sigma/\beta = 10^{-3}$.

The area of contact of rough surface features is then[29]

$$A_a = \pi^2(\xi\beta\sigma)^2 AF_2(\lambda) \tag{11}$$

$F_2(\lambda)$ is a statistical function, given as[29]

$$F_2(\lambda) = \begin{cases} \begin{Bmatrix} -0.002\lambda^5 + 0.028\lambda^4 - 0.173\lambda^3 \\ +0.526\lambda^2 - 0.804\lambda + 0.500; \end{Bmatrix} & for\ \lambda \leqslant 3 \\ 0; & for\ \lambda > 3 \end{cases} \tag{12}$$

A tribo-film of lubricant additives usually forms on the contacting surfaces. This ultra-thin film shears in a non-Newtonian manner at the limiting shear stress of the lubricant, thus[31]

$$f_{bo} = \tau_L A_a \tag{13}$$

where, τ_L is the limiting shear stress of lubricant defined as[31,32]

$$\tau_L = \tau_{0L} + \varepsilon P_m \tag{14}$$

where $P_m = \frac{W_a}{A_a}$ is the average pressure at tip of asperities and ε is the pressure-induced shear coefficient.

Evans and Johnson[33] presented a formula for viscous friction for these cases, also including the effect of generated heat. Based on their model, viscous friction can be obtained as

$$f_v = F_{flank}\left(0.87\alpha\tau_0 + 1.74\frac{\tau_0}{\bar{p}}ln\left(\frac{1.2}{\tau_0 h_{c0}}\left(\frac{2\dot{K}\eta_0}{1 + 9.6\zeta}\right)^{1/2}\right)\right) \tag{15}$$

where

$$\zeta = \frac{4}{\pi}\frac{\dot{K}}{h_{c0}/R}\left(\frac{\bar{p}}{E'RK'\rho'c'V}\right)^{1/2} \tag{16}$$

Then, the frictional power loss becomes

$$PL = f\Delta V \tag{17}$$

It is clear that the above procedure depends on the prediction of the lubricant film thickness in the contact of all the meshing gear teeth pairs. An analytical approach for this is based on the use of numerically

obtained oil film thickness formulae through regression analyses. It is important to employ an appropriate formula, applicable for the correct contact configuration and one whose basis envelopes contact kinematics and applied loads determined by TCA. 'In the case studied here the following formula is used[34]

$$h_{c0}^* = 4.31 U_e^{0.68} G_e^{0.49} W_e^{-0.073} \left\{ 1 - \exp\left[-1.23 \left(\frac{R_y}{R_x} \right)^{2/3} \right] \right\}$$

(18)

The dimensionless parameters are

$$W_e = \frac{\pi F_{flank}}{2 E_r R^2}, \quad U_e = \frac{\pi \eta_0 V}{4 E_r R}, \quad G_e = E' \alpha \quad \text{and} \quad h_{c0}^* = \frac{h_{c0}}{R}$$

where F_{flank} is the normal contact load at the mesh point, E' is the reduced elastic modulus of contacting surfaces, R is the radii of curvature at the point of contact, η_0 is the lubricant atmospheric dynamic viscosity, V is the speed of lubricant entraining motion into the contact, α is the lubricant pressure viscosity coefficient and h_{c0} is the central contact lubricant film thickness.

Applied torque

The instantaneous total resisting torque on the carrier is

$$T_c = T_w + T_{fr} \tag{19}$$

where T_w is the applied resistive torque, resident on the carrier, resulting from the longitudinal vehicle dynamics. This is measured from the track test at the JCB.

T_{fr} is the friction torque, obtained from the power loss as

$$T_{fr} = \frac{PL_T}{\dot{\theta}_c} \tag{20}$$

At a given vehicle speed, a sufficient applied torque to the sun gear maintains the steady-state conditions

$$T_s = \frac{T_c}{R_{plan}} \tag{21}$$

The calculated resistive torque from equation (19) and the driving torque from equation (21) are directly supplied to the equations of motion (equation (1)), where R_{plan} is the transfer ratio, which alters according to different configurations. The kinematic relationship between planetary gears is

$$(Z_r + Z_s)\dot{\theta}_c = \dot{\theta}_r Z_r + \dot{\theta}_s Z_s \tag{22}$$

When a gearing component is stationary, then its velocity is set to zero. Therefore, in order to maintain steady state conditions, the required torque resident on the input shaft is obtained from equations (21) and (22). For example, for the case of $\dot{\theta}_r = 0$, using equation (22) the transfer ratio becomes: $R_{plan} = \frac{Z_s}{(Z_r + Z_s)}$.

Results and discussion

The wheel hub planetary gear set of the JCB Max-Trac rear differential is studied here. The effect of mesh phasing between different branches on the efficiency and NVH of the wheel hub is considered. These planetary gear sets contribute to the NVH and efficiency of the axle during the various road testing drive cycles. Therefore, the study takes into account various load–speed combinations. The input torque to the sun gear from the differential is 609 Nm at the speed of 906 r/min. The ring gear is fixed onto the axle housing and the power is transmitted to the wheels through the carrier. The gear data are listed in Table 1. Table 2 lists the lubricant properties.

When all the planet gears make simultaneous contact at the same position along the meshing cycle with the ring and sun gears, the planetary system is in-phase as shown in Figure 3(b). A phase difference can be obtained by installing the planets at different circumferential positions. The resultant out-of-balance should be countered by additional balancing mass. The additional mass is desired in the construction machinery

Table 1. The gearbox data.

Radius of sun gear	0.026 [m]
Radius of planet gear	0.043 [m]
Radius of ring gear	0.115 [m]
Pressure angle	20°
Helix angle	0°
Number of teeth for sun gear	15
Number of teeth for planet gear	25
Number of teeth for ring gear	66
Number of planet branches	3
Moment of inertia of the sun gear	0.00035 [Kg − m⁻¹]
Moment of inertia of the planet gear	0.0016 [Kg − m⁻¹]
Moment of inertia of the carrier (including vehicle equivalent inertia)	775.4 [Kg − m⁻¹]

Table 2. Lubricant rheology.

|	
Pressure viscosity coefficient	2.38×10^{-8} [Pa⁻¹]
Atmospheric dynamic viscosity	0.0144 [Pa.s]
Eyring shear stress	2 [MPa]
Thermal conductivity	0.16 [W/m.K]
Pressure-induced shear coefficient (ε)	0.047

for operational stability under the loading and re-handling conditions. Figure 4 shows how the planet phasing affects the variation in the effective meshing stiffness of a planet–ring, and planet–sun gear contacts. It should be noted that in practice there is always a small amount of inadvertent phasing in the system assembly due to the manufacturing and assembly errors, as well as due to the assembly compliance. Therefore, understanding the effect of phasing is not only essential for tuning the system in terms of the NVH refinement and efficiency, but it is also required to investigate the effect of any undesired phasing.

In order to investigate the effect of phasing, one branch is considered as the reference (e.g. $\varnothing_{rp1} = \varnothing_{sp1} = 0$). This reference branch is considered to have 0% phase difference and the phase of other branches are measured with respect to it. The phase difference for the other two branches is considered to reside from 0% to 100% of the meshing period (Figure 3).

The meaning of 0% is that there is no phase difference with the reference branch. One hundred percent means that the specific branch has phase difference of one complete meshing cycle, which is effectively same with 0%. All possible combinations of phasing are considered in the current analysis. As a measure of NVH refinement, the peak-to-peak amplitude of the *DTE* is examined. Larger peak-to-peak amplitudes correspond to increased variations in the teeth pair contact force, which may be as the result of impact and separation (loss of friction). The resulting vibrations can induce structure-borne noise. Impacting pairs can also cause pressure perturbations, leading to airborne noise emission.
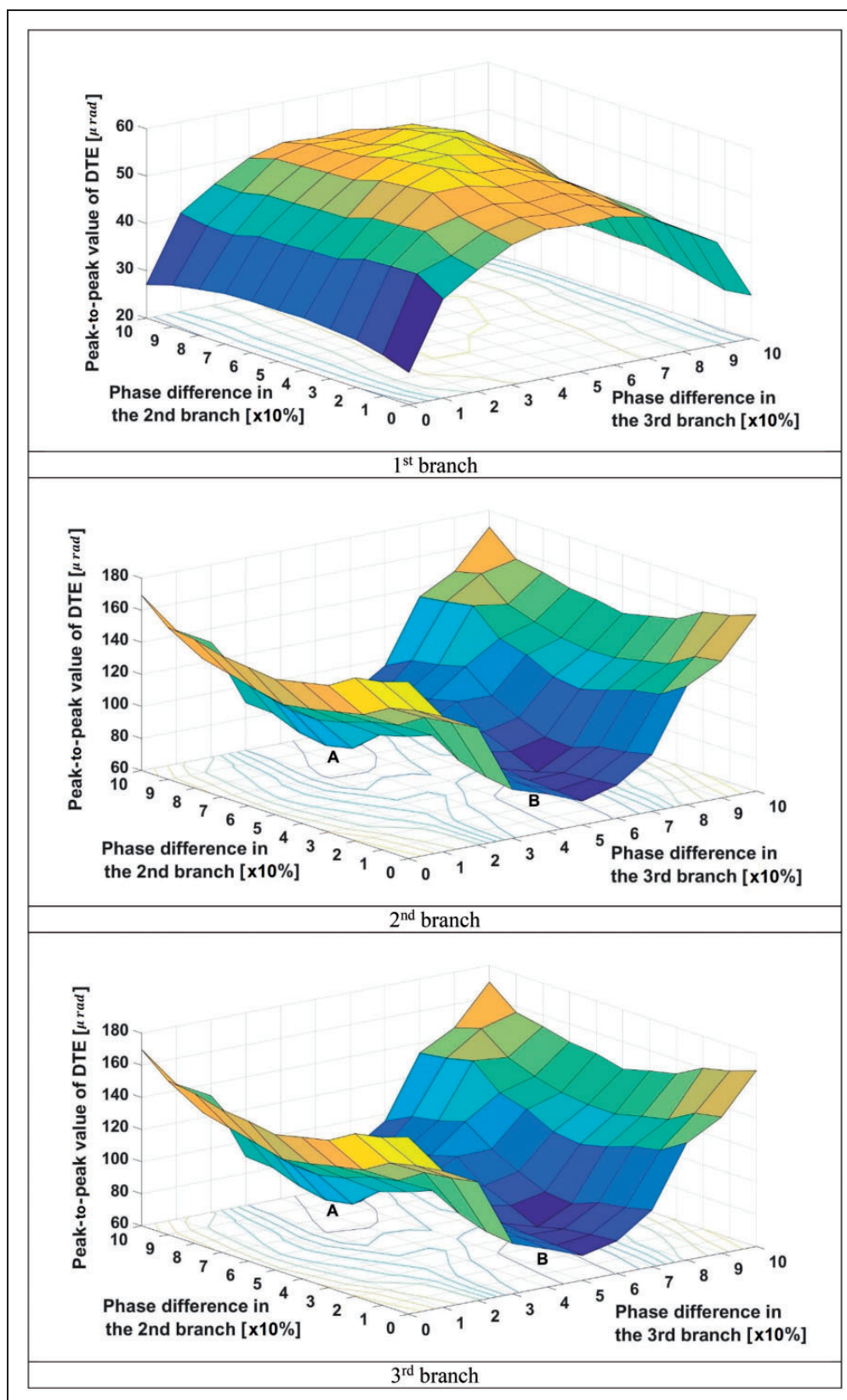
Effect of phase difference on DTE of ring–planet contacts

Figure 5 shows the *DTE* of ring–planet for an in-phase planet-branching configuration. Positive
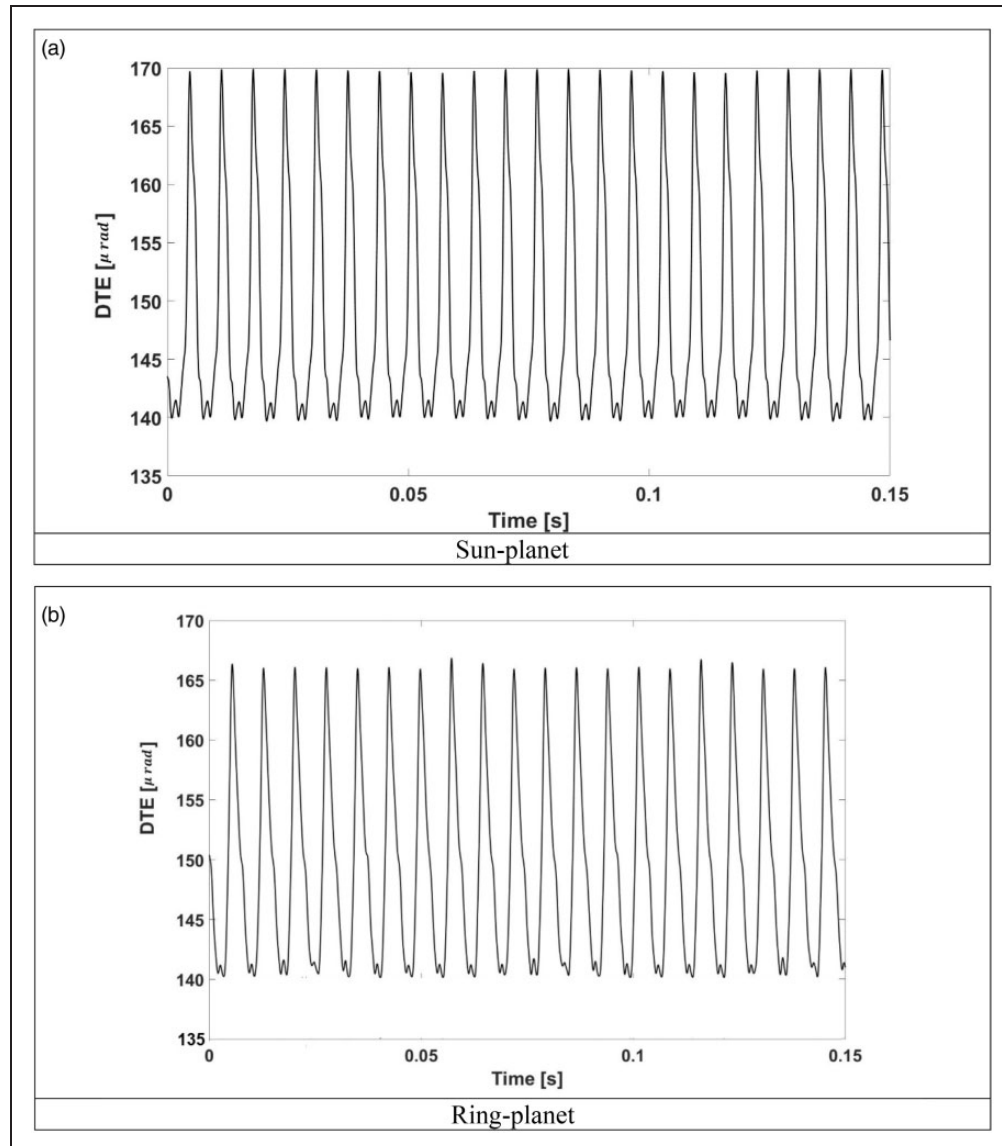
Figure 4. *DTE* of sun–planet and ring–planet with no phase difference between the branches.

Figure 5. Peak-to-peak *DTE* of ring–planet contacts for different branches and for all phasing combinations.

values of *DTE* correspond to loaded contacts with elastic deformation of the contiguous surfaces. The value of $DTE = 0$ indicates the threshold for loss of contact. Therefore, $DTE < 0$ loss of contact

occurs, which also corresponds to no traction. Under these conditions, there is no friction and the excess energy would manifest itself in the form of vibratory motion. Therefore, loss of contact or

separation is another measure of NVH refinement. As Figure 4 shows, there is no separation under the current studied working conditions.

Figure 5 shows the peak-to-peak value of the *DTE* for different combinations of phasing in branches 1, 2 and 3. The figure relates to the ring–planet contact. No teeth pair separation occurs in the contacts. The figure shows that the peak-to-peak value of the *DTE* in the ring–planet contact can be reduced by 53–57%. The minimum value for branch 1
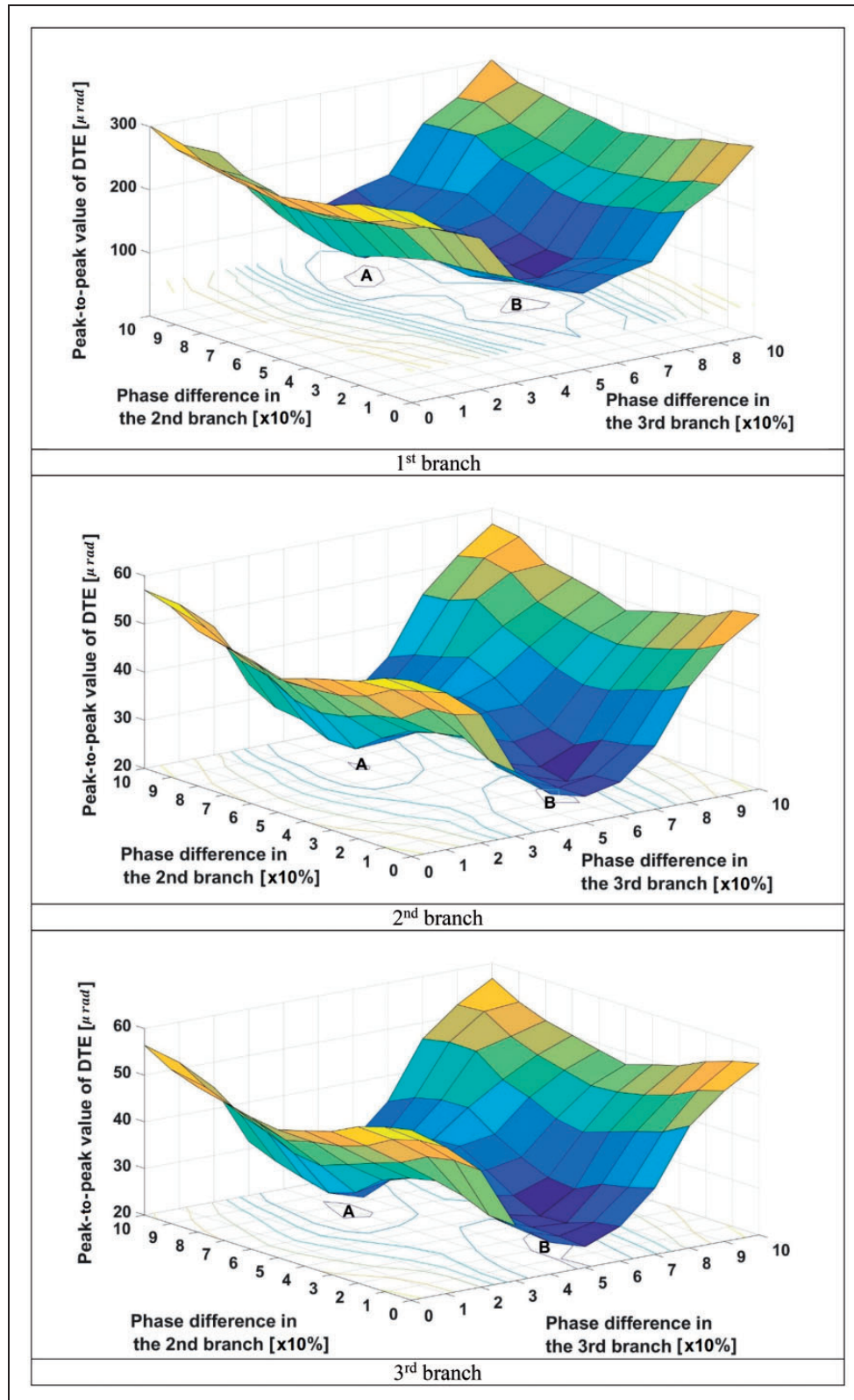
Figure 6. The peak–peak value of DTE of sun–planet contacts for different branches and for all combinations of phase differences.

can be obtained with no phase difference between all the branches. In branch 2, the minimum peak-to-peak value takes place at two positions marked by A and B in the figure. Point A is when the branches 2 and 3 have 80% and 40% phase differences, respectively. Point B takes place when the branches 2 and 3 have 30% and 60% phase differences, respectively. Considering the discrete nature of the simulations and 10% intervals between different data points, it can be concluded that the minimum DTE occurs when one of the branches has 30–40% and the other 60–80% phase difference. From practical point of view, it should be noted that 100% of phase difference can be obtained by displacing the mesh point equivalent to the complete meshing cycle. For the presented case study, this value is 14.4° of rotation of planet, which can be implemented by repositioning the carrier arm by 5.4°. On the other hand, there is an assembly constraint for planetary gear sets, which specifies

possible phase differences Ø as

$$\frac{\varnothing(Z_s + Z_r)}{360} = Integer \tag{23}$$

In the presented case study, the closest possible phase difference value to the optimum point is 4.4°, which can still provide high NVH refinement.

Very similar reduction is observed for the DTE for branch 3. Therefore, points A and B can be chosen as the optima in terms of NVH refinement. They provide 56–58% reduction in the peak-to-peak value of DTE, which requires a compromise in terms of a 50% increase in the DTE for the first branch.

For design purposes and using the current model, a multi-objective optimization can be employed with the peak-to-peak DTE for the three branches as the objective functions. Then, an optimum point can be obtained amongst all the possible combinations of phase differences.
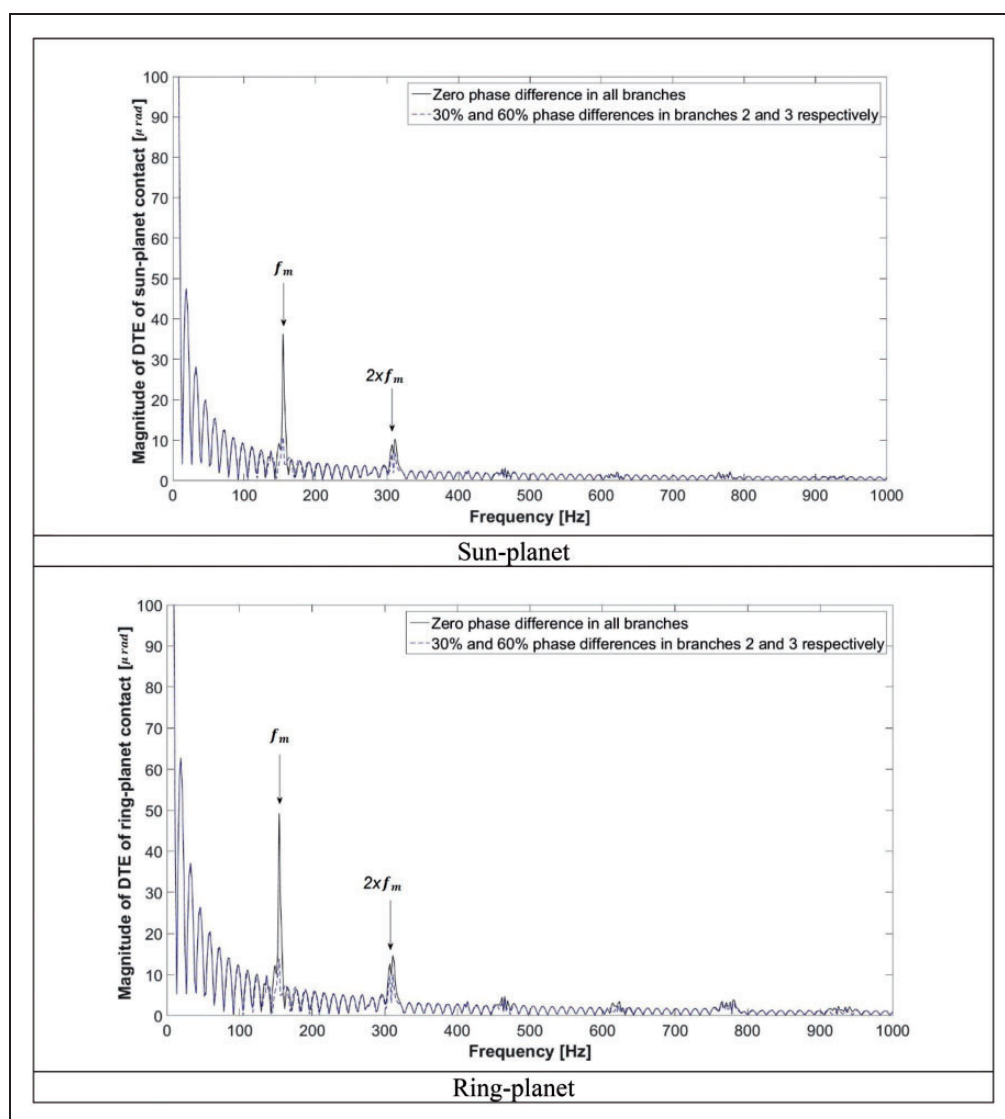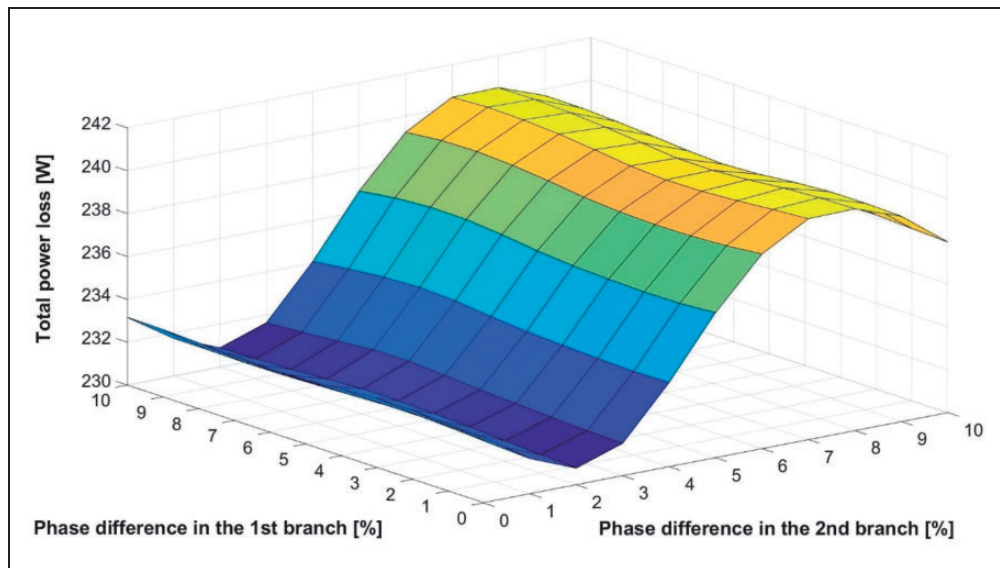

Figure 7. Spectra of sun–planet and ring–planet DTE in the branch 2.

Figure 8. Total power loss for all combinations of phase differences.

Effect of phase difference on DTE of sun–planet contacts

Figure 6 shows similar values to those in Figure 5, but related to the sun–planet contact. Again no teeth pair separation is observed under the simulated conditions. In all the branches, a reduction of 58–70% can be obtained by choosing the phase difference combinations at points A and B. These points correspond to similar conditions for points A and B in Figure 5. In the case of sun–planet contact, a consistent reduction is observed for all the branches, thus compromising for higher peak-to-peak value for one of ring–planet contacts can be justified even without any detailed optimization. In Figure 6, the reduction in the first branch is much larger than the other two branches. Noting an increase in the oscillations of the ring–planet contact of the same branch, it can be concluded that the vibratory energy is shifted to the ring–planet contact since these contacts act as parallel equivalent springs.

Effect of phase difference on specific mode shapes and total power loss

It is important to be able to target-specific mode shapes in the development process. The *DTE* is the source of excitation in the gear train system. Therefore, it is important to determine its spectral content as shown in Figure 7 for both the sun–planet and the ring–planet contacts in branch 2. The two main spectral contributions are the first and second meshing orders. In both cases, these peaks are significantly reduced with appropriate phasing as shown in the figure. This is equivalent to 25% for the first meshing order and 40% for the second meshing order.

Figure 8 shows the total power loss for all the meshing gears for different phase differences in branches 2 and 3. This shows that the power loss varies by 5% for these different combinations. The minimum power loss occurs when the phase difference in branch 2 is 20%. This minimum value is 1% lower than the original gearing configuration with no phase difference in any of the branches. However, it would be more of interest to measure the power loss at points A and B in Figures 5 and 6. This would enable a comparison for the potential improvements in NVH refinement. Point A and B show 2.4% and 0.6% higher power loss in comparison with the no-phase difference condition. This shows that the most efficient combination does not correspond to the most NVH-refined case. However, any significant improvement in the NVH refinement can justify a small loss in transmission efficiency, particularly because the latter is already at 99.6%.

Conclusion

The paper presents analysis of planetary wheel hub gears of off-highway vehicles. NVH refinement and improved transmission efficiency are the key desired attributes. Optimal conditions with these attributes do not often coincide under various operating conditions. Whilst, the primary aim is to develop an ECO-friendly and high-efficiency system, the NVH performance is also a growing area of concern.

Wheel hub planetary gears are often subject to poor NVH under the harsh operating conditions. An optimum simultaneous solution for both reduced power loss and improved NVH should be sought.

The results show that with mesh phasing of the system planetary branches such an approach can lead to near simultaneous optimal solution with respect to efficiency and NVH performance can be obtained. This alleviates the need for more costly palliative measures, such as gear teeth modification

and attainment of high manufacturing and assembly precisions. As the transmission efficiency is already quite high for planetary system, the focus of investigation can be put upon NVH assessment, whilst ensuring that mesh phasing does not adversely affect system efficiency.

The paper also shows that with such an approach, the need for detailed multi-parameter optimisation can be alleviated, at least for prescribed broad range of vehicle use. The current analysis deals with torsional system dynamics. The effect of phasing on lateral oscillations of the system should be investigated, including misalignment and supporting bearing losses.

Declaration of Conflicting Interests

The author(s) declared no potential conflicts of interest with respect to the research, authorship, and/or publication of this article.

Funding

References

1. Talbot DC, Kahraman A and Singh A. An experimental investigation of the efficiency of planetary gear sets. *Trans ASME J Mech Design* 2012; 134: 021003.
2. Kahraman A and Vijayakar S. Effect of internal gear flexibility on the quasi-static behavior of a planetary gear set. *Trans ASME J Mech Design* 2001; 123: 408–415.
3. Kahraman A. Planetary gear train dynamics. *Trans ASME J Mech Design* 1994; 116: 713–720.
4. Ambarisha VK and Parker RG. Nonlinear dynamics of planetary gears using analytical and finite element models. *J Sound Vibration* 2007; 302: 577–595.
5. Ambarisha VK and Parker RG. Suppression of planet mode response in planetary gear dynamics through mesh phasing. *Trans ASME J Vib Acoustics* 2006; 128: 133–142.
6. Bahk CJ and Parker RG. Analytical investigation of tooth profile modification effects on planetary gear dynamics. *Mech Mach Theory* 2013; 70: 298–319.
7. Talbot DC, Kahraman A and Singh A. An experimental investigation of the efficiency of planetary gear sets. *Trans ASME J Mech Design* 2012; 134: 021.
8. Mohammadpour M, Theodossiades S, Rahnejat H, et al. Transmission efficiency and noise, vibration and harshness refinement of differential hypoid gear pairs. *Proc IMechE, Part K: J Multi-body Dynamics* 2014; 228: 19–33.
9. Velex P and Cahouet V. Experimental and numerical investigations on the influence of tooth friction in spur and helical gear dynamics. *Trans ASME J Mech Design* 2000; 122: 515–522.
10. De la Cruz M, Chong WWF, Teodorescu M, et al. Transient mixed thermo-elastohydrodynamic lubrication in multi-speed transmissions. *Trib Int* 2012; 49: 17–29.
11. Mohammadpour M, Theodossiades S and Rahnejat H. Transient mixed non-Newtonian thermo-elastohydrodynamics of vehicle differential hypoid gears with starved partial counter-flow inlet boundary. *Proc IMechE, Part J: J Engineering Tribology* 2014; 228: 1158–1173.
12. Mohammadpour M, Theodossiades S and Rahnejat H. Dynamics and efficiency of planetary gear sets for hybrid powertrains. *Proc IMechE, Part C: J Mechanical Engineering Science* 2015; 230: 1359–1368.
13. Tangasawi O, Theodossiades S and Rahnejat H. Lightly loaded lubricated impacts: idle gear rattle. *J Sound Vibrat* 2007; 308: 418–430.
14. Russo R, Brancati R and Rocca E. Experimental investigations about the influence of oil lubricant between teeth on the gear rattle phenomenon. *J Sound Vibrat* 2009; 321: 647–661.
15. De la Cruz M, Theodossiades S and Rahnejat H. An investigation of manual transmission drive rattle. *Proc IMechE, Part K: J Multi-body Dynamics* 2010; 224: 167–181.
16. Koronias G, Theodossiades S, Rahnejat H, et al. Axle whine phenomenon in light trucks: a combined numerical and experimental investigation. *Proc IMechE, Part D: J Automobile Engineering* 2011; 225: 885–894.
17. Chen Z and Shao Y. Dynamic simulation of planetary gear with tooth root crack in ring gear. *Eng Failure Anal* 2013; 31: 8–18.
18. Sun T and Hu H. Nonlinear dynamics of a planetary gear system with multiple clearances. *Mech Machine Theory* 2003; 38: 1371–1390.
19. Spitas C and Spitas V. Coupled multi-DOF dynamic contact analysis model for the simulation of intermittent gear tooth contacts, impacts and rattling considering backlash and variable torque. *Proc IMechE, Part C: J Mechanical Engineering Science* 2016; 230: 1022–1047.
20. Inalpolat M and Kahraman A. Dynamic modelling of planetary gears of automatic transmissions. *Proc IMechE, Part K: J Multi-body Dynamics* 2008; 222: 229–242.
21. Iglesias M, del Rincon AF, de-Juan A, et al. Advanced model for the calculation of meshing forces in spur gear planetary transmissions. *Meccanica* 2015; 50: 1869–1894.
22. Iglesias M, del Rincon AF, de-Juan A, et al. Planetary transmission load sharing: manufacturing errors and system configuration study. *Mech Machine Theory* 2017; 111: 21–38.
23. Oyague F. *Gearbox modeling and load simulation of a baseline 750-kW wind turbine using state-of-the-art simulation codes*. Golden, CO: National Renewable Energy Laboratory, 2009.
24. Vijayakar S. *CALYX manual*. Columbus, OH: Advanced Numerical Solutions, 2000.
25. Xu H and Kahraman A. Prediction of friction-related power losses of hypoid gear pairs. *Proc IMechE, Part K: J Multi-body Dynamics* 2007; 221: 387–400.
26. Karagiannis I, Theodossiades S and Rahnejat H. On the dynamics of lubricated hypoid gears. *Mech Mach Theory* 2012; 48: 94–120.
27. Dietl P, Wensing J and Van Nijen GC. Rolling bearing damping for dynamic analysis of multi-body systems-experimental and theoretical results. *Proc IMechE, Part K: J Multi-body Dynamics* 2000; 214: 33–43.

28. Mohammadpour M, Theodossiades S and Rahnejat H. Multi-physics investigations on the dynamics of differential hypoid gears. *Trans ASME J Vibration Acoust* 2014; 136: 041007.

29. Greenwood JA and Tripp JH. The contact of two nominally flat rough surfaces. *Proc IMechE, Part C: J Mechanical Engineering Science* 1970–1971; 185: 625–633.

30. Gohar R and Rahnejat H. *Fundamentals of tribology*. London: Imperial College Press, 2008.

31. Johnson KL and Cameron R. Fourth paper: shear behaviour of elastohydrodynamic oil films at high rolling contact pressures. *Proc IMechE, Part C: J Mechanical Engineering Science* 1967; 182: 307–330.

32. Mohammadpour M, Theodossiades S, Rahnejat H, et al. Non-Newtonian mixed elastohydrodynamics of differential hypoid gears at high loads. *Meccanica* 2014; 49: 1115–1138.

33. Evans CR and Johnson KL. Regimes of traction in elastohydrodynamic lubrication. *Proc IMechE, Part C: J Mechanical Engineering Science* 1986; 200: 313–324.

34. Chittenden RJ, Dowson D, Dunn JF, et al. A theoretical analysis of the isothermal elastohydrodynamic lubrication of concentrated contacts II. General case, with lubricant entrainment along either principal axis of the Hertzian contact ellipse or at some intermediate angle. *Proc R Soc Ser A* 1985; 397: 271–294.

Appendix

Notation

A	apparent contact area
A_a	contact area of asperities
B	backlash
c	damping coefficient
c'	thermal capacity of conjunctional solids
E'	effective modulus of elasticity
f	friction
f_{bo}	boundary friction
f_m	meshing frequency
f_v	viscous friction
F_{flank}	flank load
h_{c0}	lubricant film thickness at the centre of contact
I	polar moment of inertia
$\dot{K}$	conductivity of the lubricant
K'	conductivity of solid bodies
k	stiffness
$\bar{p}$	average contact pressure
PL	power loss
R	contact radii of curvature
r	radii of meshing teeth
T	torque
V	lubricant entrainment velocity
ΔV	sliding velocity
W_a	load carried by asperities
Z	number of teeth
α	pressure–viscosity coefficient
β	asperity tip radius
ε	pressure-induced shear coefficient of bounding surfaces
η_0	lubricant ambient dynamic viscosity
θ	torsional degrees of freedom
λ	stribeck oil film parameter
ρ'	density of contacting solids
σ	composite surface roughness of contacting surfaces
τ_L	limiting shear stress of the lubricant
τ_0	Eyring shear stress
τ_{L0}	limiting shear stress at ambient pressure
$\emptyset$	phase difference

Subscripts

bo	denotes boundary lubrication regime
c	belongs to carrier
p	denotes planet
$plan$	planetary gears
r	ring gear
rp	ring-to-planet
s	sun gear
sp	sun-to-planet
T	total
v	viscous
w	wheel